Intercalation of Si between MoS$_2$ layers

Rik van Bremen[‡1], Qirong Yao[‡1], Soumya Banerjee[2], Deniz Cakir[2], Nuri Oncel[2]
and Harold J. W. Zandvliet[*1]

Full Research Paper

Abstract

We report a combined experimental and theoretical study of the growth of sub-monolayer amounts of silicon (Si) on molybdenum disulfide (MoS$_2$). At room temperature and low deposition rates we have found compelling evidence that the deposited Si atoms intercalate between the MoS$_2$ layers. Our evidence relies on several experimental observations: (1) Upon the deposition of Si on pristine MoS$_2$ the morphology of the surface transforms from a smooth surface to a hill-and-valley surface. The lattice constant of the hill-and-valley structure amounts to 3.16 Å, which is exactly the lattice constant of pristine MoS$_2$. (2) The transitions from hills to valleys are not abrupt, as one would expect for epitaxial islands growing on-top of a substrate, but very gradual. (3) $I(V)$ scanning tunneling spectroscopy spectra recorded at the hills and valleys reveal no noteworthy differences. (4) Spatial maps of dI/dz reveal that the surface exhibits a uniform work function and a lattice constant of 3.16 Å. (5) X-ray photo-electron spectroscopy measurements reveal that sputtering of the MoS$_2$/Si substrate does not lead to a decrease, but an increase of the relative Si signal. Based on these experimental observations we have to conclude that deposited Si atoms do not reside on the MoS$_2$ surface, but rather intercalate between the MoS$_2$ layers. Our conclusion that Si intercalates upon the deposition on MoS$_2$ is at variance with the interpretation by Chiappe et al. (*Adv. Mater.* **2014,** *26,* 2096–2101) that silicon forms a highly strained epitaxial layer on MoS$_2$. Finally, density functional theory calculations indicate that silicene clusters encapsulated by MoS$_2$ are stable.

Introduction

Since the discovery of graphene [1-4] interest has extended to the search for other 2D materials with properties similar to graphene. One appealing candidate is silicene, a graphene-like 2D allotrope of silicon. The first calculations of graphite-like allotropes of silicon and germanium were performed by Takeda and Shiraishi in 1994 [5]. These authors pointed out that two-dimensional silicon and germanium are not planar but buckled, i.e., the two sub-lattices of the honeycomb lattice are displaced with respect to each other in a direction normal to the two-dimensional sheet. In addition, the calculations of Takeda and

Shiraishi [5] also revealed that silicene and germanene are semi-metals, like graphene. In 2007, Guzmán-Verri and Lew Yan Voon [6] performed tight-binding calculations of two-dimensional silicon. They pointed out that the graphite-like silicon sheet has linearly dispersing energy bands near the *K* points of the Brillouin zone, very comparable to graphene. Inspired by this analogy they put forward the name silicene for the two-dimensional silicon. Interestingly, the linear dispersing energy bands at the *K* points, the so-called Dirac cones, are robust against the buckling of the silicene lattice [5,7]. In 2009, Cahangirov et al. [7] found that germanene also exhibits similar properties as graphene and silicene.

Similar to graphene, the electrons near the Fermi level in free-standing silicene are predicted to behave as massless Dirac fermions [6]. The broken sub-lattice symmetry of silicene allows for the opening of a band gap in this material [8-12]. This band gap makes silicene a very appealing candidate for field-effect-based devices. Another attractive property of silicene is its spin–orbit coupling, which is substantially larger than the spin–orbit coupling in graphene [13,14].

Silicene does not occur in nature and therefore it has to be synthesized. Several studies have reported on the growth of a 2D silicon layer on Ag(111) [15-17]. Unfortunately, due to the strong coupling between Si ad-layer and Ag substrate, the interesting Dirac properties of silicene are destroyed [18]. Although a linear dispersion relation has been observed [17], it is argued by others that this band is related to the Ag substrate rather than to silicene [19] or to combined effects of silicene and the Ag(111) substrate [20,21]. Growth of silicon was also demonstrated on graphite, a van der Waals material, with the idea to suppress the interaction with the substrate and as such to preserve the Dirac properties [22]. Unfortunately, graphite is metallic, which could also affect the electronic bands of silicene in the vicinity of the Fermi level. Van der Waals materials with a band gap do not suffer from this limitation. Molybdenum disulfide (MoS_2) is a member of the transition metal dichalcogenide (TMD) family that belongs to the class of van der Waals materials. Bulk MoS_2 has a band gap of 1.29 eV, which increases to 1.90 eV for a monolayer of MoS_2 [23]. This means that MoS_2 has no states near the Fermi level and therefore hybridization with the energy bands of silicene near the Fermi level cannot occur. Recently, germanene, a 2D allotrope of germanium [24-28], has already been successfully grown on MoS_2 [29]. Chiappe et al. [30] deposited Si on MoS_2 and found that Si forms an epitaxially strained layer on top of MoS_2 with a lattice constant identical to the MoS_2 lattice constant, i.e., 3.16 Å. A study confirming the two-dimensionality of deposited Si on MoS_2 has recently been carried out using variable-angle X-ray photoelectron spectroscopy (XPS) [31]. It should be pointed out here that this study showed that the S $2p_{3/2}$ peak in MoS_2 is at around 167.6 eV, which is considerably higher than the pure core-level line of pure S. This high value might be an indication of contamination with O [32] or Ni [33].

Here we revisit the growth of Si on MoS_2. Our scanning tunneling microscopy (STM) observations are very similar to those reported by Chiappe et al. [30]. However, we arrive at the conclusion that Si intercalates between the MoS_2 layers. In order to verify our conclusion we have performed additional spectroscopic measurements. These additional spectroscopic measurements unambiguously reveal that sub-monolayer amounts of Si deposited on MoS_2 at room temperature do not reside on top of MoS_2, but intercalate between the MoS_2 layers.

Experimental

The scanning tunneling microscopy and spectroscopy measurements were performed with an Omicron STM-1 room-temperature scanning tunneling microscope in ultra-high vacuum (UHV). The UHV system is composed of three separate chambers: a load-lock chamber for a quick entry of new samples and STM tips, a preparation chamber with facilities for sample heating, ion bombardment and evaporation of silicon and an STM chamber. The base pressures in the STM chamber and the preparation chamber are below 3×10^{-11} mbar and 5×10^{-11} mbar, respectively. The MoS_2 samples are purchased from HQ graphene. Prior to inserting the samples into the lock-load system they were cleaned by mechanical exfoliation. Silicon was deposited on the MoS_2 samples using a custom-built Si evaporator, which consists of a small piece of a Si wafer that can be heated resistively. The distance between substrate and evaporator is about 10 cm. The silicon was deposited at a rather low deposition rate of 0.8 nm·h^{-1}. The silicon evaporator was calibrated by depositing a sub-monolayer amount of Si on a Ge(001) substrate. The Ge(001) surface was cleaned by applying several cycles of Ar ion sputtering and annealing. After deposition and mild annealing at a temperature of 450–500 K, the Ge(001) substrate was inserted into the STM and subsequently the areal coverage of the epitaxial Si islands was determined. *I*(*V*) curves are recorded at constant height at 450 ms per curve. Spatial maps of d*I*/d*z* are measured using a lock-in amplifier. A small high frequency (ca. 1.9 kHz) sinusoidal signal is added to the *z*-piezo and the tunnel current is fed into the lock-in amplifier. The output signal of the lock-in amplifier, which is proportional to d*I*/d*z*, is measured simultaneously with the topography.

MoS_2 samples used for the X-ray photoelectron spectroscopy (XPS) experiments were purchased from nanoScience Instruments. The MoS_2 samples were exfoliated before Si deposition. In a separate UHV chamber, Si was deposited on the MoS_2

sample via resistive heating of a small piece of a silicon wafer and then the MoS$_2$ sample was quickly transferred to the XPS chamber. During this transfer the sample was exposed to ambient conditions. The deposited amount of Si was 0.5 monolayers. The base pressure of both chambers is below 4×10^{-10} mbar. Both MoS$_2$ and Si/MoS$_2$ samples were measured with a monochromatic Al Kα (1486.6 eV) X-ray source with a pass energy of 89.5 eV and 35.75 eV for survey and high-resolution scans, respectively. During the XPS measurements, the pressure was kept at or below 1×10^{-9} mbar. The angle between the X-ray source, which is aligned along the surface normal, and spectrometer is 54.7°. All XPS core-level spectra were analyzed using Augerscan software, which is equipped with its own curve-fitting program. The core-level peaks are fitted using a Gaussian–Lorentzian (GL) function to include the instrumental response function along with the core-level line shape. The secondary-electron background was subtracted using a Shirley function [34]. The energy differences between the 3d and 2p spin–orbit couples were set to 3.13 eV and 1.18 eV, respectively. The ratios of the areas of the doublet peaks were also fixed. During sputtering the pressure is increased to 3×10^{-8} mbar by leaking in Ar gas while the pressure around the filament in the differentially pumped argon gas chamber increased to 1×10^{-4} mbar. The sample was sputtered with a beam of Ar ions with 1 kV energy. The emission current used was 25 mA, which resulted in an ion current of 0.33 μA.

The shape of the beam is circular with a diameter of approximately 2 mm.

First-principles calculations are based on the projector-augmented wave (PAW) method [35,36] within DFT as implemented in the Vienna ab initio simulation package (VASP) [37]. The exchange–correlation interactions are treated using the generalized gradient approximation (GGA) within the Perdew–Burke–Ernzerhof (PBE) formulation [38]. The plane waves are expanded with an energy cut of 400 eV. Since the semi-local functionals, such as GGA, fail to describe weakly interacting systems, we also take into account the van der Waals interaction [39,40]. Brillouin-zone integrations for structure relaxations are approximated by using the special *k*-point sampling of the Monkhorst–Pack scheme with a Γ-centered $3 \times 3 \times 1$ grid [41]. In order to minimize the periodic interactions along the *z*-direction (the direction perpendicular to the plane of the hetero-trilayer) the vacuum space between the layers has a width of at least 15 Å.

Results and Discussion

In Figure 1, STM images of pristine MoS$_2$ and MoS$_2$ after the deposition of ca. 0.2 monolayers of Si at room temperature are shown. The pristine MoS$_2$ surface appears very smooth. Usually only the top sulfur layer is resolved, resulting in a lattice with hexagonal symmetry and a lattice constant of 3.16 Å (see
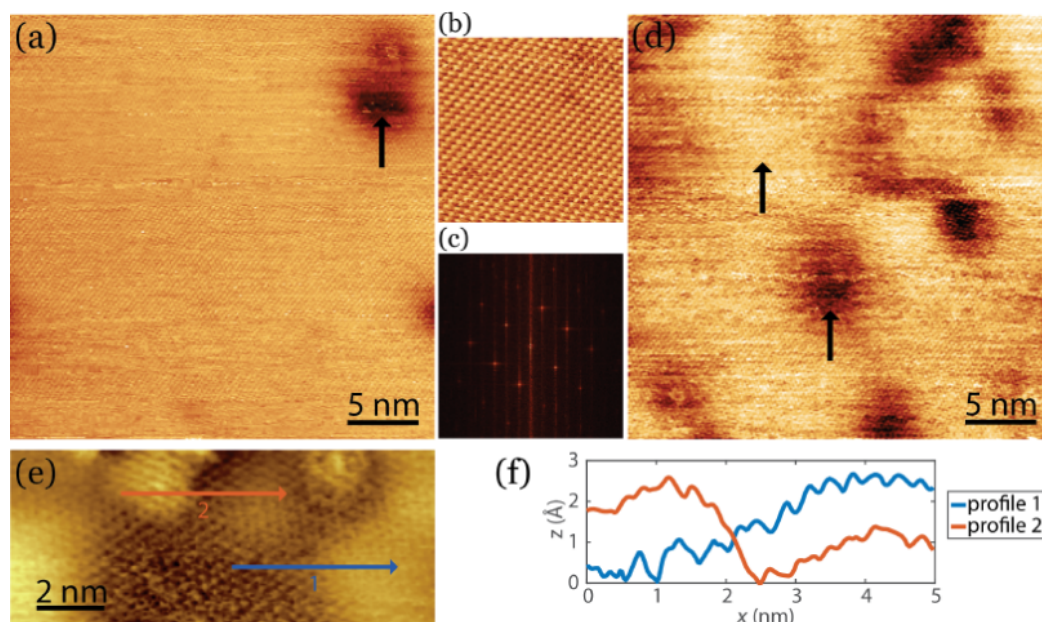

Figure 1: (a) STM image of pristine MoS$_2$ taken prior to the deposition of Si. The arrow indicates an intrinsic defect, which is often found on MoS$_2$. (b) High-resolution STM image of pristine MoS$_2$. (c) Fast Fourier-transform of pristine MoS$_2$ showing the hexagonal symmetry. (d) STM image taken after the deposition of 0.2 monolayers of Si. The arrows indicate a hill (bright) and a valley (dark). (e) High-resolution STM image taken after the deposition of 0.2 monolayers of Si. (f) Line scans taken along the lines indicated in panel (e). The sample bias is 1.2V and the tunnelling current is 0.5 nA.

Figure 1b,c). The pristine MoS$_2$ contains some intrinsic defects, which are visible as dark depressions as indicated by the arrow in Figure 1a. These defects are most probably caused by vacancies or interstitials and have been found to exhibit a metal-like behavior [42,43]. Upon the deposition of 0.2 monolayers of Si, the surface morphology converts to a hill-and-valley structure as shown in Figure 1d. The arrows indicate a bright hill and a dark valley. Upon further deposition of silicon, the surface becomes rougher and more difficult to scan as shown in Figure S1 in Supporting Information File 1. When even more silicon is deposited, silicon clusters on top of MoS$_2$ become visible. A close-up image of the transition of a hill to a valley is represented in Figure 1e. The line profiles indicated in the figure correspond to the cross sections shown in Figure 1f. The typical height variation of a transition is found to be of several angstroms. We found a similar height variation using density functional theory (DFT) calculations of the intercalation of a single silicon layer in between two MoS$_2$ layers. These calculations are discussed after the presentation of the experimental results. It is immediately obvious from Figure 1f that the transition from a hill to a valley is very gradual. Interestingly, the lattice constant of the hill-and-valley structure is identical to the lattice constant of pristine MoS$_2$, i.e. 3.16 Å. Both observations are similar to the observations reported by Chiappe et al. [30] who deposited 0.8 monolayers of silicon on MoS$_2$ (obtained from SPI) at 200 °C. Based on these observations Chiappe et al. [30] concluded that Si grows epitaxially on MoS$_2$ with a lattice constant that is identical to MoS$_2$. This implies that the Si layer is highly strained, indicative of a rather strong interaction between MoS$_2$ and Si. This seems unlikely, bearing in mind that MoS$_2$ is a van der Waals material. We tentatively put forward another interpretation, namely that Si intercalates between the MoS$_2$ layers. The gradual transition from a hill to a valley as well as the observation of the MoS$_2$ lattice constant after Si deposition nicely fits into this picture.

In order to verify our interpretation we have performed additional scanning tunneling spectroscopy (STS) measurements. $I(V)$ scanning tunneling spectra were recorded at the hills and valleys as indicated by the arrows in Figure 1d. Average spectroscopy curves of a hill and of a valley, which in total are comprised of 3500 spectra, are displayed in Figure 2. The $I(V)$ spectra are almost identical to each other. The small difference between both curves might be a residual effect of Si residing underneath the MoS$_2$ layer. If the top layer were a silicon cluster the $I(V)$ spectra would differ significantly as is shown in Figure S2 in Supporting Information File 1.
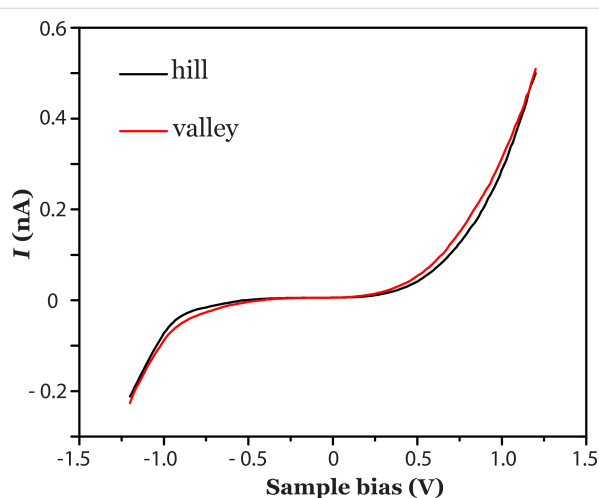

Figure 2: STS recorded at the hills (black curve) and at the valleys (red curve). Set points sample bias 1.2 V and tunnel current 0.5 nA.

In order to remove the large-scale height variation from the topography scan, we simultaneously recorded a spatial map of dI/dz (Figure 3). The dI/dz signal only depends on the effective work function, also referred to as the apparent barrier height, and not on any large-scale height variations [44,45]. It should
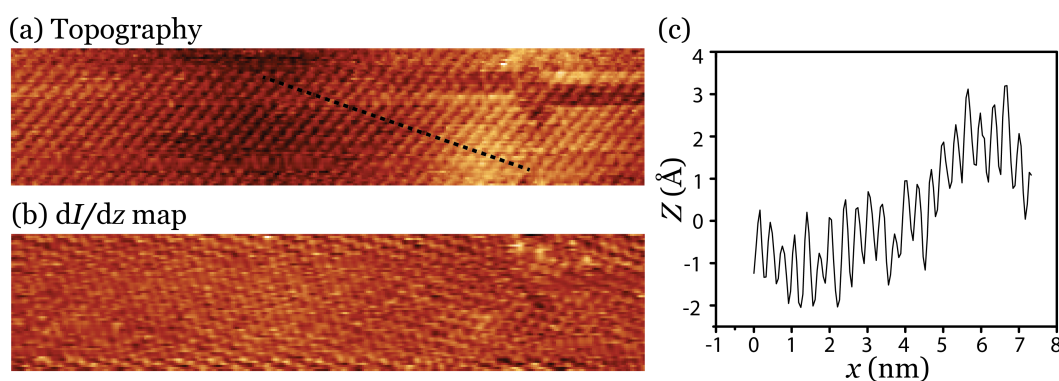

Figure 3: (a) STM image of a MoS$_2$ surface after the deposition of 0.2 monolayers of Si. (b) Spatial map of dI/dz. In both images the atomic structure is resolved. (c) Line- scan taken along the dotted line depicted in panel (a). Sample bias is 1.2 V and tunnel current is 0.5 nA.

be pointed out here that spatial maps of dI/dz often exhibit a resolution that is similar to normal topographic STM images without, of course, the large-scale height variations [44].

The results shown in Figure 3 make clear two points. First, since height information is not present in a dI/dz map we have to conclude that the surface is smooth and continuous. Second, dI/dz provides information on the apparent barrier height, which is a material property. No contrast is visible and therefore we have to conclude that we are dealing with the same material, i.e., MoS_2. Both these points provide compelling evidence that the deposited Si intercalates between the MoS_2 layers. For a comparable system, namely Si on WSe_2, we recently arrived at a similar conclusion [45].

XPS measurements have been performed to obtain insight of the chemical composition of the top layers. Before depositing Si, XPS measurements were carried out on pristine MoS_2 in order to find the exact positions of the Mo $3d_{5/2}$ and S $2p_{3/2}$ core-level peaks. (Figure 4a and Figure 4b, respectively). The Mo $3d_{5/2}$ and S $2p_{3/2}$ peaks were measured at 230.25 eV and 163.09 eV, respectively. The location of these peaks is in good agreement with [46,47].

The core-level spectra of Si, Mo and S after the deposition of 0.5 monolayers of Si on MoS_2 are shown in Figure 5a, Figure 5b and Figure 5c, respectively. A higher coverage than in the case of STM is used in order to yield a stronger signal in the XPS measurements. STM topography images with a higher coverage can be found in Figure S1 in Supporting Information File 1. The XPS data show two peaks associated with Si. The smaller peak, located at 98.13 eV, can be attributed to pristine

Si. The other peak, measured at 103 eV, can be attributed to oxidized silicon [48]. The oxidation of Si occurs during the transfer of the sample from the growth chamber to the XPS chamber. During this transfer the sample was exposed to ambient conditions. A more detailed analysis reveals that only 5% of the Si is pristine, whereas the rest is oxidized. Upon sputtering of the MoS_2/Si sample with an Ar ion beam with 1 kV energy, we observe that the relative Si signal increases while the relative S signal decreases as can be seen in Figure S3 in Supporting Information File 1. This observation indicates that Si has intercalated between the MoS_2 layers. In addition, we also conclude that the intercalated Si can be oxidized.

It is well known that numerous elements have a strong tendency to intercalate between MoS_2 layers [49,50]. As for the intercalation mechanism of silicon in between MoS_2 layers, we can only speculate. A plethora of studies on the intercalation of different chemical species in TMDs have been reported from elements as small as lithium [51], sodium [52-54] and carbon [55] to elements as large as cesium [56,57] and gold [58]. Other studies report on the intercalation of silicon and other elements under graphene layers synthesized on metal substrates [59-61].

The driving force for intercalation is charge transfer between the intercalated atoms and the layered material [62,63] or thermodynamic stabilization [61,62]. The mechanism of intercalation was found to occur through cracks and wrinkles in the layers [60] and via edges [51]. Because the diffusion barrier of adsorbed silicon atoms on top of MoS_2 is assumed to be very low and the experiments are performed at room temperature, it is expected that silicon adatoms can easily diffuse over the surface to reach these cracks, wrinkles and step edges.
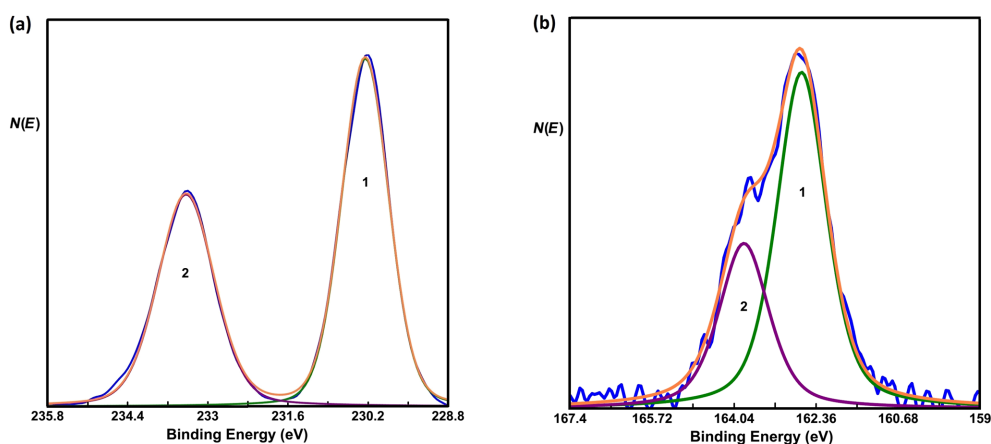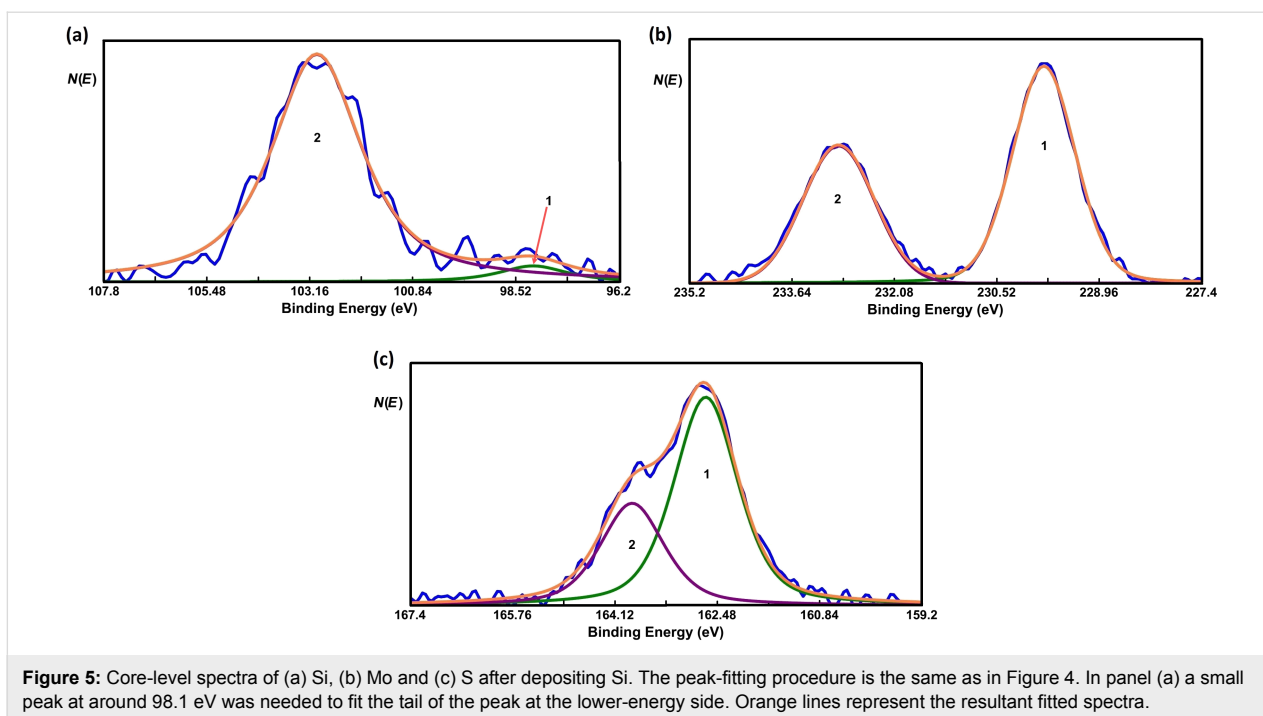

Figure 4: Core-level spectra of (a) Mo and (b) S before depositing Si. The spectra are fitted with two GL function peaks. In (a), 1 and 2 represent the Mo $3d_{5/2}$ and $3d_{3/2}$ peaks, respectively. In (b), 1 and 2 represent the S $2p_{3/2}$ and $2p_{1/2}$ peaks, respectively. In both figures, the resultant fitted spectra are represented by an orange line.

Figure 5: Core-level spectra of (a) Si, (b) Mo and (c) S after depositing Si. The peak-fitting procedure is the same as in Figure 4. In panel (a) a small peak at around 98.1 eV was needed to fit the tail of the peak at the lower-energy side. Orange lines represent the resultant fitted spectra.

In order to study the effect of the oxidation of intercalated silicon in more detail we measured the exact positions of the Mo $3d_{5/2}$ and S $2p_{3/2}$ peaks. Both peaks shift to a lower binding energy by about 0.45 eV. This shift cannot be interpreted as a simple chemical shift due to a chemical reaction of the involved elements, i.e., Mo/S/Si and O [64]. In addition, after the deposition of Si no significant changes in the FWHM of the peaks of Mo (0.97 before, 1.13 after) as well as of S (1.09 before, 1.21 after) were observed, indicating that no chemical reaction between MoS_2 and silicon oxide has occurred. It is very likely that the observed shift is attributed to a change in the position of the Fermi level.

It has been shown that the deposition of MoS_2 on a SiO_2 substrate with interface impurities leads to a charge transfer from the MoS_2 surface to the defect states and, thus, to the formation of surface dipoles [65]. These dipoles shift the Fermi level of MoS_2 closer to the valence band maximum (p-type). The shift of the Fermi level also leads to a shift in the binding energy of the Mo and S peaks to lower binding energies.

Next, we will discuss the results of our density functional theory calculations regarding the intercalated Si. To be consistent with experimental results we have fixed the lattice constant of MoS_2 to 3.16 Å. We first calculated the structural and electronic properties of hetero-trilayers composed of a silicene layer intercalated between two MoS_2 monolayers (MoS_2–silicene–MoS_2). Due to the large lattice mismatch, we have considered a commensurable supercell, in which we have

placed a 5 × 5 silicene cell and a 6 × 6 MoS_2 cell on top of each other. For this configuration the lattice mismatch of the MoS_2–silicene–MoS_2 trilayer becomes less than 1%. Figure 6 shows the optimized structure of the MoS_2–silicene–MoS_2 hetero-trilayer. The calculated interlayer distance in a pristine
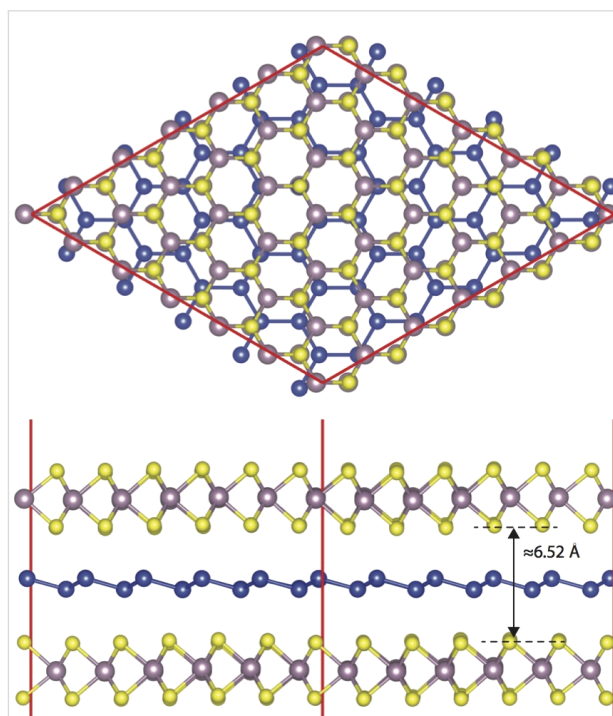

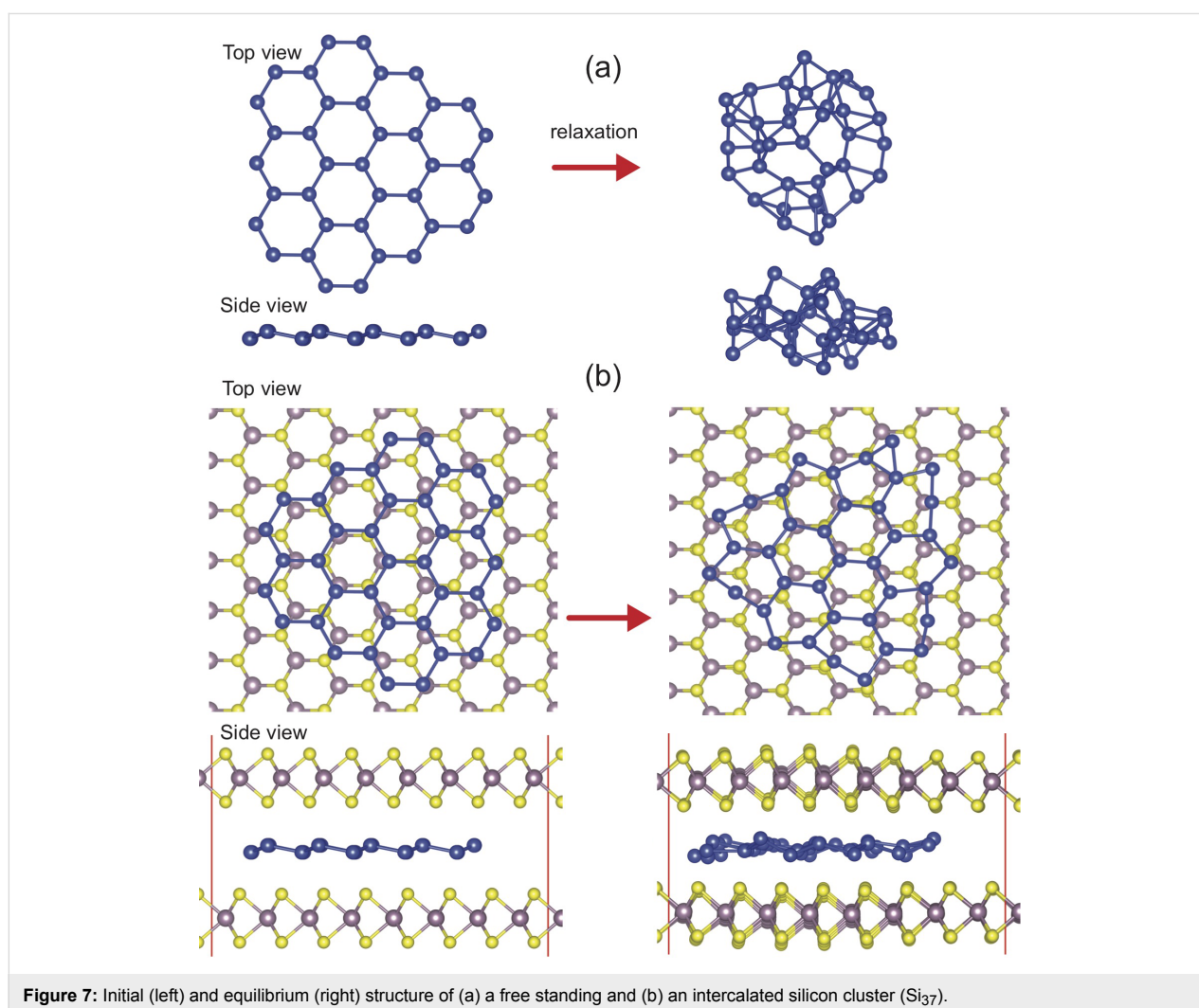**Figure 6:** Top and side views of silicene intercalated in bilayer MoS_2.

MoS_2 bilayer is found to be 3.00 Å. Insertion of a silicene monolayer enlarges the interlayer separation between MoS_2 layers from 3 Å to 6.52 Å, corresponding to an increase of the interlayer separation of 3.52 Å.

In order to study the possible formation of silicene between the MoS_2 monolayers, we consider a buckled 2D silicon cluster (Si_{37}) consisting of six-membered silicon rings. We used a 7×7 super-cell structure for the MoS_2 bilayer. Initial and equilibrium geometries for both a free-standing as well as the intercalated silicon cluster inserted between the MoS_2 layers are shown in Figure 7. We found that a free-standing 2D buckled silicon cluster is, in contrast to an infinite silicene layer, not even metastable in vacuum and spontaneously transforms into a strongly buckled 3D assembly as seen in Figure 7a. The intercalated silicon cluster in Figure 7b also undergoes a remarkable structural reconstruction. The optimized structure of a silicon cluster encapsulated between two MoS_2 layers is totally different from the free-standing optimized silicon cluster in vacuum.

This is noticeable in that the shape of the hexagons is not uniform as is the case for silicene. Especially at the edges, due to the presence of the Si dangling bonds, the hexagons are seriously distorted. However, intercalation between MoS_2 layers preserves the 2D buckled structure of the silicon cluster during the structure relaxation. Thus, we suggest that the intercalation of silicon atoms between MoS_2 layers may promote the formation of silicene, which interacts only weakly with the environment via van der Waals forces. We found that both top and bottom MoS_2 layers develop bumps due to the interaction with the silicon cluster. The average interlayer MoS_2 distance varies within the range of 5.5–6.2 Å, which corresponds to an increase in interlayer separation of 2.5-3.2 Å. This agrees well with the measured height variation.

Conclusion

In this work we revisited the growth of Si on MoS_2. STM topography data reveals that Si does not grow on top of the MoS_2 substrate, but rather intercalates in between the MoS_2 layers. It

Figure 7: Initial (left) and equilibrium (right) structure of (a) a free standing and (b) an intercalated silicon cluster (Si_{37}).

is known that layered materials such as MoS_2 have a tendency to host intercalants. In this work we provide additional evidence for silicon intercalation by using STS and XPS. Since silicon intercalates it is interesting to scrutinize if there are possibilities to grow a 2D layer in between two layers of MoS_2. Our density functional theory calculations show that 2D silicon clusters intercalated between MoS_2 layers are stable.

Supporting Information

Supporting Information File 1
Additional experimental data.
[http://www.beilstein-journals.org/bjnano/content/supplementary/2190-4286-8-196-S1.pdf]

Acknowledgements

References

1. Novoselov, K. S.; Geim, A. K.; Morozov, S. V.; Jiang, D.; Zhang, Y.; Dubonos, S. V.; Grigorieva, I. V.; Firsov, A. A. *Science* **2004,** *306,* 666–669. doi:10.1126/science.1102896
2. Zhang, Y.; Tan, Y.-W.; Stormer, H. L.; Kim, P. *Nature* **2005,** *438,* 201–204. doi:10.1038/nature04235
3. Ohta, T.; Bostwick, A.; Seyller, T.; Horn, K.; Rotenberg, E. *Science* **2006,** *313,* 951–954. doi:10.1126/science.1130681
4. Castro Neto, A. H.; Guinea, F.; Peres, N. M. R.; Novoselov, K. S.; Geim, A. K. *Rev. Mod. Phys.* **2009,** *81,* 109–162. doi:10.1103/RevModPhys.81.109
5. Takeda, K.; Shiraishi, K. *Phys. Rev. B* **1994,** *50,* 14916–14922. doi:10.1103/PhysRevB.50.14916
6. Guzmán-Verri, G. G.; Lew Yan Voon, L. C. *Phys. Rev. B* **2007,** *76,* 075131. doi:10.1103/PhysRevB.76.075131
7. Cahangirov, S.; Topsakal, M.; Aktürk, E.; Şahin, H.; Ciraci, S. *Phys. Rev. Lett.* **2009,** *102,* 236804. doi:10.1103/PhysRevLett.102.236804
8. Song, Y.-L.; Zhang, S.; Lu, D.-B.; Xu, H.-r.; Wang, Z.; Zhang, Y.; Lu, Z.-W. *Eur. Phys. J. B* **2013,** *86,* 488. doi:10.1140/epjb/e2013-31078-4
9. Quhe, R.; Fei, R.; Liu, Q.; Zheng, J.; Li, H.; Xu, C.; Ni, Z.; Wang, Y.; Yu, D.; Gao, Z.; Lu, J. *Sci. Rep.* **2012,** *2,* 853. doi:10.1038/srep00853
10. Ni, Z.; Liu, Q.; Tang, K.; Zheng, J.; Zhou, J.; Qin, R.; Gao, Z.; Yu, D.; Lu, J. *Nano Lett.* **2012,** *12,* 113–118. doi:10.1021/nl203065e
11. Gao, N.; Li, J. C.; Jiang, Q. *Phys. Chem. Chem. Phys.* **2014,** *16,* 11673. doi:10.1039/C4CP00089G
12. Drummond, N. D.; Zólyomi, V.; Fal'ko, V. I. *Phys. Rev. B* **2012,** *85,* 075423. doi:10.1103/PhysRevB.85.075423
13. Kane, C. L.; Mele, E. J. *Phys. Rev. Lett.* **2005,** *95,* 226801. doi:10.1103/PhysRevLett.95.226801
14. Lew Yan Voon, L. C. *Chin. Phys. B* **2015,** *24,* 087309. doi:10.1088/1674-1056/24/8/087309
15. Lalmi, B.; Oughaddou, H.; Enriquez, H.; Kara, A.; Vizzini, S.; Ealet, B.; Aufray, B. *Appl. Phys. Lett.* **2010,** *97,* 223109. doi:10.1063/1.3524215
16. Jamgotchian, H.; Colignon, Y.; Hamzaoui, N.; Ealet, B.; Hoarau, J. Y.; Aufray, B.; Bibérian, J. P. *J. Phys.: Condens. Matter* **2012,** *24,* 172001. doi:10.1088/0953-8984/24/17/172001
17. Vogt, P.; De Padova, P.; Quaresima, C.; Avila, J.; Frantzeskakis, E.; Asensio, M. C.; Resta, A.; Ealet, B.; Le Lay, G. *Phys. Rev. Lett.* **2012,** *108,* 155501. doi:10.1103/PhysRevLett.108.155501
18. Lin, C.-L.; Arafune, R.; Kawahara, K.; Kanno, M.; Tsukahara, N.; Minamitani, E.; Kim, Y.; Kawai, M.; Takagi, N. *Phys. Rev. Lett.* **2013,** *110,* 076801. doi:10.1103/PhysRevLett.110.076801
19. Chen, M. X.; Weinert, M. *Nano Lett.* **2014,** *14,* 5189–5193. doi:10.1021/nl502107v
20. Feng, Y.; Liu, D.; Feng, B.; Liu, X.; Zhao, L.; Xie, Z.; Liu, Y.; Liang, A.; Hu, C.; Hu, Y.; He, S.; Liu, G.; Zhang, J.; Chen, C.; Xu, Z.; Chen, L.; Wu, K.; Liu, Y.-T.; Lin, H.; Huang, Z.-Q.; Hsu, C.-H.; Chuang, F.-C.; Bansil, A.; Zhou, X. J. *Proc. Natl. Acad. Sci. U. S. A.* **2016,** *113,* 14656–14661. doi:10.1073/pnas.1613434114
21. Fleurence, A.; Friedlein, R.; Ozaki, T.; Kawai, H.; Wang, Y.; Yamada-Takamura, Y. *Phys. Rev. Lett.* **2012,** *108,* 245501. doi:10.1103/PhysRevLett.108.245501
22. De Crescenzi, M.; Berbezier, I.; Scarselli, M.; Castrucci, P.; Abbarchi, M.; Ronda, A.; Jardali, F.; Park, J.; Vach, H. *ACS Nano* **2016,** *10,* 11163–11171. doi:10.1021/acsnano.6b06198
23. Mak, K. F.; Lee, C.; Hone, J.; Shan, J.; Heinz, T. F. *Phys. Rev. Lett.* **2010,** *105,* 136805. doi:10.1103/PhysRevLett.105.136805
24. Li, L.; Lu, S.; Pan, J.; Qin, Z.; Wang, Y.; Wang, Y.; Cao, G.; Du, S.; Gao, H.-J. *Adv. Mater.* **2014,** *26,* 4820–4824. doi:10.1002/adma.201400909
25. Dávila, M. E.; Xian, L.; Cahangirov, S.; Rubio, A.; Le Lay, G. *New J. Phys.* **2014,** *16,* 095002. doi:10.1088/1367-2630/16/9/095002
26. Bampoulis, P.; Zhang, L.; Safaei, A.; van Gastel, R.; Poelsema, B.; Zandvliet, H. J. W. *J. Phys.: Condens. Matter* **2014,** *26,* 442001. doi:10.1088/0953-8984/26/44/442001
27. Zhang, L.; Bampoulis, P.; van Houselt, A.; Zandvliet, H. J. W. *Appl. Phys. Lett.* **2015,** *107,* 111605. doi:10.1063/1.4931102
28. Acun, A.; Zhang, L.; Bampoulis, P.; Farmanbar, M.; van Houselt, A.; Rudenko, A. N.; Lingenfelder, M.; Brocks, G.; BPoelsema, K.; atsnelson, M. I.; Zandvliet, H. J. W. *J. Phys.: Condens. Matter* **2015,** *27,* 443002. doi:10.1088/0953-8984/27/44/443002
29. Zhang, L.; Bampoulis, P.; Rudenko, A. N.; Yao, Q.; van Houselt, A.; Poelsema, B.; Katsnelson, M. I.; Zandvliet, H. J. W. *Phys. Rev. Lett.* **2016,** *116,* 256804. doi:10.1103/PhysRevLett.116.256804
30. Chiappe, D.; Scalise, E.; Cinquanta, E.; Grazianetti, C.; van den Broek, B.; Fanciulli, M.; Houssa, M.; Molle, A. *Adv. Mater.* **2014,** *26,* 2096–2101. doi:10.1002/adma.201304783
31. Molle, A.; Lamperti, A.; Rotta, D.; Fanciulli, M.; Cinquanta, E.; Grazianetti, C. *Adv. Mater. Interfaces* **2016,** *3,* 1500619. doi:10.1002/admi.201500619
32. Wagner, C. D.; Taylor, J. A. *J. Electron Spectrosc. Relat. Phenom.* **1982,** *28,* 211–217. doi:10.1016/0368-2048(82)85044-5
33. Yu, X.-R.; Liu, F.; Wang, Z.-Y.; Chen, Y. *J. Electron Spectrosc. Relat. Phenom.* **1990,** *50,* 159–166. doi:10.1016/0368-2048(90)87059-W

34. Briggs, D.; Seah, M. P. *Practical Surface Analysis by Auger and X-Ray Photoelectron Spectroscopy;* John Wiley & Sons Ltd: New York, NY, U.S.A., 1983.

35. Kresse, G.; Furthmüller, J. *Phys. Rev. B* **1996,** *54,* 11169–11186. doi:10.1103/PhysRevB.54.11169

36. Blöchl, P. E. *Phys. Rev. B* **1994,** *50,* 17953–17979. doi:10.1103/PhysRevB.50.17953

37. Kresse, G.; Joubert, D. *Phys. Rev. B* **1999,** *59,* 1758–1775. doi:10.1103/PhysRevB.59.1758

38. Perdew, J. P.; Burke, K.; Ernzerhof, M. *Phys. Rev. Lett.* **1996,** *77,* 3865–3868. doi:10.1103/PhysRevLett.77.3865

39. Grimme, S.; Antony, J.; Ehrlich, S.; Krieg, H. *J. Chem. Phys.* **2010,** *132,* 154104. doi:10.1063/1.3382344

40. Grimme, S.; Ehrlich, S.; Goerigk, L. *J. Comput. Chem.* **2011,** *32,* 1456–1465. doi:10.1002/jcc.21759

41. Monkhorst, H. J.; Pack, J. D. *Phys. Rev. B* **1976,** *13,* 5188–5192. doi:10.1103/PhysRevB.13.5188

42. Addou, R.; Colombo, L.; Wallace, R. M. *ACS Appl. Mater. Interfaces* **2015,** *7,* 11921–11929. doi:10.1021/acsami.5b01778

43. Bampoulis, P.; van Bremen, R.; Yao, Q.; Poelsema, B.; Zandvliet, H. J. W.; Sotthewes, K. *ACS Appl. Mater. Interfaces* **2017,** *9,* 19278–19286. doi:10.1021/acsami.7b02739

44. Wiesendanger, R. *Scanning Probe Microscopy and Spectroscopy: Methods and Applications;* Cambridge University Press: Cambridge, United Kingdom, 1994. doi:10.1017/CBO9780511524356

45. Yao, Q.; van Bremen, R.; Zandvliet, H. J. W. *Appl. Phys. Lett.* **2016,** *109,* 243105. doi:10.1063/1.4972036

46. Lince, J. R.; Carré, D. J.; Fleischauer, P. D. *Effects of Argon-Ion Bombardment on the Basal Plan Surface of MoS2 – Report Sd-TR-86-95;* Space Division, Air Force Systems Command: Los Angeles, CA, U.S.A., 1987.

47. Vissers, J. P. R.; Groot, C. K.; van Oers, E. M.; Beer, D.; Prins, R. *Bull. Soc. Chim. Belg.* **1984,** *93,* 813–822. doi:10.1002/bscb.19840930822

48. Finster, J.; Klinkenberg, E.-D.; Heeg, J.; Braun, W. *Vacuum* **1990,** *41,* 1586–1589. doi:10.1016/0042-207X(90)94025-L

49. Benavente, E.; Santa Ana, M. A.; Mendizábal, F.; González, G. *Coord. Chem. Rev.* **2002,** *224,* 87–109. doi:10.1016/S0010-8545(01)00392-7

50. Vázquez, A. *Mater. Lett.* **1998,** *35,* 22–27. doi:10.1016/S0167-577X(97)00224-3

51. Xiong, F.; Wang, H.; Liu, X.; Sun, J.; Brongersma, M.; Pop, E.; Cui, Y. *Nano Lett.* **2015,** *15,* 6777–6784. doi:10.1021/acs.nanolett.5b02619

52. Brauer, H. E.; Ekvall, I.; Olin, H.; Starnberg, H. I.; Wahlström, E.; Hughes, H. P.; Strocov, V. N. *Phys. Rev. B* **1997,** *55,* 10022. doi:10.1103/PhysRevB.55.10022

53. Brauer, H. E.; Starnberg, H. I.; Holleboom, L. J.; Strocov, V. N.; Hughes, H. P. *Phys. Rev. B* **1998,** *58,* 10031–10045. doi:10.1103/PhysRevB.58.10031

54. Ekvall, I.; Brauer, H. E.; Wahlström, E.; Olin, H. *Phys. Rev. B* **1999,** *59,* 7751. doi:10.1103/PhysRevB.59.7751

55. Kwieciñski, W.; Sotthewes, K.; Poelsema, B.; Zandvliet, H. J. W.; Bampoulis, P. *J. Colloid Interface Sci.* **2017,** *505,* 776–782. doi:10.1016/j.jcis.2017.06.076

56. Pettenkofer, C.; Jaegermann, W.; Schellenberger, A.; Holub-Krappe, E.; Papageorgopoulos, C. A.; Kamaratos, M.; Papageorgopoulos, A. *Solid State Commun.* **1992,** *84,* 921–926. doi:10.1016/0038-1098(92)90459-M

57. Starnberg, H. I.; Brauer, H. E.; Holleboom, L. J.; Hughes, H. P. *Phys. Rev. Lett.* **1993,** *70,* 3111–3114. doi:10.1103/PhysRevLett.70.3111

58. Iyikanat, F.; Sahin, H.; Senger, R. T.; Peeters, F. M. *APL Mater.* **2014,** *2,* 092801. doi:10.1063/1.4893543

59. Meng, L.; Wu, R.; Zhou, H.; Li, G.; Zhang, Y.; Li, L.; Wang, Y.; Gao, H.-J. *Appl. Phys. Lett.* **2012,** *100,* 083101. doi:10.1063/1.3687688

60. Petrović, M.; Šrut Rakić, I.; Runte, S.; Busse, C.; Sadowski, J. T.; Lazić, P.; Pletikosić, I.; Pan, Z.-H.; Milun, M.; Pervan, P.; Atodiresei, N.; Brako, R.; Šokčević, D.; Valla, T.; Michely, T.; Kralj, M. *Nat. Commun.* **2013,** *4,* 2772. doi:10.1038/ncomms3772

61. Li, G.; Zhou, H.; Pan, L.; Zhang, Y.; Huang, L.; Xu, W.; Du, S.; Ouyang, M.; Ferrari, A. C.; Gao, H.-J. *J. Am. Chem. Soc.* **2015,** *137,* 7099–7103. doi:10.1021/ja5113657

62. Whittingham, M. S.; Chianelli, R. R. *J. Chem. Educ.* **1980,** *57,* 569. doi:10.1021/ed057p569

63. Odink, D. A.; Song, K.; Kauzlarich, S. M. *Chem. Mater.* **1992,** *4,* 906–911. doi:10.1021/cm00022a029

64. NIST X-ray Photoelectron Spectroscopy (XPS) Database, Version 3.5. https://srdata.nist.gov/xps/Default.aspx (accessed June 27, 2017).

65. Dolui, K.; Rungger, I.; Sanvito, S. *Phys. Rev. B* **2013,** *87,* 165402. doi:10.1103/PhysRevB.87.165402